HHS Public Access

Author manuscript

Angiogenesis. Author manuscript; available in PMC 2021 November 19.

Published in final edited form as:

Angiogenesis. 2020 August ; 23(3): 443–458. doi:10.1007/s10456-020-09723-z.

Endothelial deletion of ADAM10, a key regulator of Notch signaling, causes impaired decidualization and reduced fertility in female mice

Nicole Lustgarten Guahmich, BS[1,2], **Gregory Farber, PhD**[1], **Shiva Shafiei, DVM, DVSc**[3], **Dylan McNally, BS**[1], **David Redmond, PhD**[2], **Eleni Kallinos, BS**[2], **Heidi Stuhlmann, PhD**[4], **Daniel Dufort, PhD**[3], **Daylon James, PhD**[2], **Carl P. Blobel, MD, PhD**[1,5]

[1]Department of Physiology, Biophysics and Systems Biology, Weill Cornell Medicine, New York, NY

[2]Center for Reproductive Medicine and Infertility, Weill Cornell Medicine, New York, NY

[3]Research Institute of the McGill University Health Centre, Montréal, QC, Canada

[4]Department of Cell and Developmental Biology, Weill Cornell Medicine, New York, NY

[5]Arthritis and Tissue Degeneration Program, Hospital for Special Surgery, New York, NY

Abstract

During the initiation of pregnancy, the vasculature of the implantation site expands rapidly, yet little is known about this process or its role in fertility. Here, we report that endothelial-specific deletion of a disintegrin and metalloprotease 10 (ADAM10), an essential regulator of Notch signaling, results in severe subfertility in mice. We found that implantation sites develop until 5.5 days post conception (dpc) but are resorbed by 6.5 dpc in *A10ΔEC* mice. Analysis of the mutant implantation sites showed impaired decidualization and abnormal vascular patterning compared to controls. Moreover, RNA-seq analysis revealed changes in endothelial cell marker expression consistent with defective ADAM10/Notch signaling in samples from *A10ΔEC* mice, suggesting that this signaling pathways is essential for the physiological function of endometrial endothelial cells during early pregnancy. Our findings raise the possibility that impaired endothelial cell function could be a cause for Repeated Pregnancy Loss (RPL) and infertility in humans.

Corresponding Author: Dr. Carl P. Blobel, Hospital for Special Surgery at Weill Cornell Medicine, 535 East 70th, New York, NY, 10021, Ph: 212-606-1429, Fax: 212-774-2560, blobelc@hss.edu.
Research Institute of McGill University Health Center, Montreal, Canada

Author contributions. NLG, GF and CB designed the experiments and prepared the manuscript. NLG harvested all tissues, maintained the mouse colony, performed immunofluorescence experiments and histopathology analysis. EK assisted with the histopathology. NLG and DJ prepared the samples for RNA sequencing and DR and DM helped with the analysis of the RNA-seq data. DD and SS performed the artificial decidualization assays and provided valuable advice and input. HS provided guidance and intellectual input throughout the project. All authors contributed to the editing of the manuscript.

Compliance with ethical standards

Conflict of interest. The authors declare that they have no conflict of interest.

Keywords

Endothelial Cells; ADAM10 (a disintegrin and metalloprotease 10); Notch; Endometrial vasculature; Infertility; Angiogenesis; Vascular Biology; Physiology; Developmental Biology; Reproductive Biology

Introduction

During early pregnancy the uterine endometrial vasculature undergoes extensive remodeling and differentiation in order to prepare for blastocyst implantation and to support the growing embryo [1]. Blastocyst attachment and subsequent invasion into the maternal endometrium initiates the process of decidualization, which involves the differentiation of uterine stromal fibroblasts into biosynthetically active secretory cells termed decidual cells. The decidual cells and the expanding endometrial vasculature are responsible for nurturing the embryo during the early stages of development. Inadequacies in the formation of the decidua in humans have been linked to Repeated Pregnancy Loss (RPL) and placental pathologies that result in intrauterine growth restrictions later during pregnancy [2–5].

There have been significant advances in uncovering the molecular pathways involved in the differentiation of decidual cells. Follistatin has been implicated in decidualization as an upstream regulator of BMP signaling [6]. Moreover, BMP2 regulates decidualization in mice through the Msx homeobox genes [7], and Forkhead box a2 (FOXA2) has an important role in decidualization and blastocyst implantation [8]. Deletion of Notch receptors and their downstream signaling effectors using a uterine specific Progesterone Receptor (*Pgr)-Cre* system results in impaired decidualization [9–11]. Studies with a Notch signaling reporter have shown that this pathway is dynamically regulated in the maternal uterine vasculature during early pregnancy in mice [12]. In endothelial cells, Notch signaling has been implicated in the establishment of an arterial versus venous cell fate in early development and in the decision between becoming a tip versus a stalk cell during retinal angiogenesis [13–20]. However, the role of endothelial Notch signaling in the process of decidualization remains to be established.

Notch signaling is regulated by the membrane-anchored metalloprotease ADAM10, which controls both Notch1 and Notch4 signaling in endothelial cells [21–23] (reviewed in [13]). Disruptions in the ADAM10/Notch signaling pathway in endothelial cells leads to abnormalities in highly specialized vascular niches, such as the retina, kidney glomeruli, intestinal villi, liver, bone and coronary vasculature [24,25]. Since mice lacking ADAM10 in endothelial cells (*A10ΔEC*) are born at Mendelian ratios and survive into adulthood, this provided an opportunity to elucidate the contribution of endothelial ADAM10/Notch signaling to female fertility. Here, we report that female *A10ΔEC* mice have strongly reduced fertility, raising questions about the underlying mechanism. We therefore analyzed the endometrial vasculature of *A10ΔEC* mice to help understand why the lack of endothelial ADAM10 leads to early pregnancy loss and severe subfertility. Our result uncovered evidence for an essential role for ADAM10, a key regulator of Notch signaling, in the differentiation of decidual endothelial cells.

Results

A10ΔEC females suffer from severe sub-fertility

Mice lacking ADAM10 in endothelial cells (*Adam10flox/flox-Tie2-Cre,* referred to as *A10ΔEC* mice) are viable, but have a number of defects in highly specialized vascular structures (e.g. kidney glomeruli, coronary vessels, liver sinusoids, intestinal villi, retinal and bone vasculature) [24]. To determine whether fertility is affected in *A10ΔEC* female mice, 8 adult mutant mice and 8 age-matched controls (*Adam10flox/flox,* without the *Tie2-Cre* transgene) were mated with control males (*Adam10flox/flox,* no *Tie2-Cre*) for a total of 4 months (Table I). During this time, six female *A10ΔEC* mice did not give birth, whereas the remaining two had a relatively small number of offspring (a total of 9 pups or 10 pups each, over the course of three litters). On average, *A10ΔEC* females gave birth to a total of 2.3 ± 4.4 pups per mouse over 4 months, whereas control mice had a total of 22.88 ± 3.1 pups per female in this time period. Previous studies had shown that mice with two floxed alleles of ADAM10 did not display any evident pathology in the absence of a *Cre* transgene [24]. Nevertheless, to further confirm that the infertile or subfertile phenotypes were solely dependent on the maternal genotype and not on the floxed alleles of ADAM10 in the male controls, we performed additional matings with wildtype males (129S1/SvImj) and five *A10ΔEC* females for 4 months. These five *A10ΔEC* females gave birth to a total of 8 pups in two litters, with an average of 1.6 ± 2.6 pups per female over 4 months (Table I). Thus, long-term fertility tracking showed that *A10ΔEC* females are either infertile or severely subfertile.

Loss of pregnancy in *A10ΔEC* females occurs during early decidualization and is independent of ovarian function

In order to determine the time of pregnancy loss in *A10ΔEC* female mice, timed matings were performed with mutant and control females, followed by dissection of the uterine horns to count visible implantation sites at 4.5 days post conception (dpc) (n=5), 5.5 dpc (n=15) and 6.5 dpc (n=9) (Fig. 1a). These time points correspond to the implantation and early decidualization stages in murine pregnancy. Pontamine blue staining at 4.5 dpc showed no difference in implantation site number between *A10ΔEC* and control female mice. At 5.5 dpc all analyzed *A10ΔEC* female mice were pregnant, although there was a significant decrease in the number of implantation sites at 5.5 dpc in mutant compared to control females (~20% reduction). However out of the *A10ΔEC* females analyzed at 6.5 dpc, only 2 females still had implantation sites. Of these, one female showed 6 implantation sites and the second female showed 1 implantation site (representative images shown in Fig. 1a, quantification in Fig. 1b). These findings suggest that pregnancy loss in *A10ΔEC* females is accompanied by almost complete resorption of the implantation sites between 5.5 dpc and 6.5 dpc.

Before the formation of the placenta, the Corpus Luteum (CL) is responsible for progesterone production in the ovaries to prepare the uterus for embryo implantation and subsequent development of the decidua. Assessment of ovarian morphology in *A10ΔEC* females by H&E staining at 5.5 dpc showed adequate formation of the CL and comparable overall morphology of the ovaries (Fig. 2a). Moreover, we found increased levels of serum

estrogen in *A10ΔEC* females compared to wild type controls at 4.5 dpc, but comparable levels at 5.5 dpc. At both of these time points, progesterone levels were slightly, but not significantly reduced (supplementary Fig. 1). Furthermore, immunofluorescence staining for the endothelial marker CD31 showed no major difference in the appearance or distribution pattern of endothelial cells in the CL in mutants versus control females at this stage (Fig. 2b). These results suggested that the loss of pregnancy in A10ΔEC females is not a result of ovarian dysfunction but could instead be caused by a defect in the endometrial vasculature.

Implantation sites of *A10ΔEC* females have a smaller diameter, reduced primary decidual zone (pdz) area and lack of embryonic crypt formation

In mice, the attachment of the embryo to the luminal epithelium and subsequent invasion triggers the differentiation of uterine stromal cells into decidual cells. The implantation of the embryo in the anti-mesometrial side of the lumen is followed by the decidualization of the cells proximal to the implantation site, an area referred to as the primary decidual zone (pdz) [26] (Fig. 3a). A previously performed morphological assessment of a non-pregnant *A10ΔEC* uteri showed no evident differences compared to a control [24]. Furthermore, histological sections of pregnant 4.5 dpc uteri showed no major differences in the appearance of the embryos in the luminal epithelium, nor in its surrounding structures (representative example shown in supplementary Fig. 2). However, H&E staining of cross-sections of mutant implantation sites at 5.5 dpc showed that the mutant implantation sites were round instead of oval and significantly smaller compared to controls (Fig. 3b, quantification shown in c). Moreover, we observed abnormal embryonic crypt formation in *A10ΔEC* females (indicated by red arrows in Fig. 3b). The implanting embryo remained localized in the anti-mesometrial side of the lumen in mutant females, whereas it had already invaded the maternal decidua in controls at this stage (Fig. 3b). We also frequently observed enlarged spaces filled with red blood cells adjacent to the mutant implantation sites, consistent with aberrant blood vessel formation (Fig. 3b, lower panel, black arrows). Serial sections of an *A10ΔEC* and control uterus at 5.5 dpc confirm that the embryo (e) is still present in both cases and show the blood-filled spaces adjacent to the implantation site in the mutants (supplementary Fig. 3)

Since the timing of pregnancy loss in *A10ΔEC* females coincides with the initiation of the decidualization reaction, we assessed whether the endometrial stromal cells had the potential to differentiate into decidual cells. Alkaline phosphatase staining, which is a commonly used marker for differentiated decidual cells [27], was clearly visible in the implantation sites of *A10ΔEC* females at 5.5 dpc (Fig. 3d). In a normal decidualization reaction, the alkaline phosphatase positive decidual cells form a compact elliptical layer with well-defined boundaries to the implantation crypt and the anti-mesometrial side (Fig. 3d). However, in the mutant females, the decidualization reaction was less widely distributed throughout the stroma and less organized than in the controls (Fig. 3d). Overall, *A10ΔEC* females presented with smaller implantation sites and inadequate decidualization, presumably caused by an inappropriate vascular contribution to this process. However, the ability of stromal cells to differentiate into alkaline phosphatase positive cells did not appear to be affected.

Artificial decidualization of *A10ΔEC* females recapitulates the impaired decidualization phenotype

Next, we sought to determine whether the presence or absence of blastocysts affects the observed phenotype. This was addressed in a mouse model for artificial decidualization, in which *A10ΔEC* (n=8) and control females (n=8) were mated with vasectomized males to induce pseudopregnancy. At day 3.5 dpc, the formation of an artificially induced decidual reaction, which is referred to as a deciduoma, was elicited by performing a scratch along the anti-mesometrial side of the lumen of one horn. The contralateral horn served as an internal control. Four days later, the uterine horns were dissected, photographed and weighed (Fig. 4a,b). In the control group, the untreated horns appeared normal and had an average weight of 0.04g ± 0.005 g, while the decidualized horns were enlarged and weighed 0.22 ± 0.05 g, showing a significant increase in uterine horn weight upon induction of decidualization. In the *A10ΔEC* females, control horns averaged 0.03 ± 0.01 g and the decidualized horn appeared larger and showed a significant increase in weight to 0.1 ± 0.06 g. Importantly, the weights of the scratched uterine horns from *A10ΔEC* mice were significantly lower than those of the controls, corroborating that *A10ΔEC* females are able to react to artificial decidualization stimuli, yet to a substantially lesser extent than the control females (Fig. 4b). These results indicate that decidualization in *A10ΔEC* females is impaired independently of any putative embryonic signals.

Implantation sites of *A10ΔEC* females at 5.5 dpc show a disorganized vasculature with an increase in endothelial cell coverage

To investigate the possibility that deficiencies in the endometrial vasculature are the cause for infertility in *A10ΔEC* females, we characterized the changes in the vasculature from the pre-implantation period until early decidualization. Immunofluorescence staining for the pan-endothelial cell marker CD31 in the implantation sites of *A10ΔEC* females at different time points during early pregnancy (3.5 dpc, 4.5 dpc and 5.5 dpc) showed a significant increase in the area covered by CD31+ cells in the endometrium of *A10ΔEC* females at 5.5 dpc, but not at the earlier time points (Fig. 5a, bottom panels, enlargement shown in Fig. 5b, quantification in Fig. 5c). Specifically, the vessels closer to the implantation sites of *A10ΔEC* females appeared abnormally large and organized in honeycomb-like structures, which were absent in controls (Fig. 5b). Moreover, there was an accumulation of CD31+ cells surrounding the luminal epithelium and increased vascularization of the area proximal to the implantation site in the mutants, whereas the corresponding area in controls had reduced vascular density (Fig. 5a, bottom panels and b). Since the abnormal vascular patterning in *A10ΔEC* females only became apparent at 5.5 dpc, but not at 3.5 dpc or 4.5 dpc, this suggests that the defect in *A10ΔEC* females mainly affects the vascular expansion and remodeling during decidualization, but presumably not before embryonic invasion.

To further characterize the vascular phenotype in *A10ΔEC* implantation sites at 5.5 dpc, we first focused on endothelial markers of Notch signaling that are known to be dysregulated in other vascular beds in *A10ΔEC* mice [28,29]. As shown in supplementary Fig. 4a, the vessels in the mutant and wildtype endometrium stained with the venous and capillary marker Endomucin (Emcn [30–32]), including the abnormally enlarged vessels in the central decidual area surrounding the embryo in mutant mice. There was also increased

immunofluorescence staining for VEGFR2 in this area at the center of the implantation sites in *A10ΔEC* females at 5.5 dpc compared to age matched controls, consistent with the increase in vascularity. Finally, there was only minimal staining for VEGFR3 in the implantation sites of controls, but slightly more patches of localized staining of larger vessels in *A10ΔEC* implantation sites. (supplementary Fig. 4b, middle panel, pointed by white arrows). The increased Emcn and VEGFR2 staining of the enlarged abnormal vasculature surrounding the embryo in *A10ΔEC* implantation sites is consistent with a defect in endothelial ADAM10/Notch signaling.

The implantation sites of *A10ΔEC* females are perfused and display similar levels of hypoxia as controls

To determine whether perfusion of the implantation sites is affected in *A10ΔEC* females, we analyzed whole-mounts of uteri following retro-orbital perfusion with fluorescently labeled lectin at 5.5 dpc. We found that the endometrial vessels in the *A10ΔEC* females were perfused (Fig. 6a). However, the perfusion pattern differed from controls in that it mimicked the vascular abnormalities described above, with increased lectin accumulation closer to the site of embryo implantation in the mutant (Fig. 6a). Staining for the epithelial marker E-cadherin helped identify the embryonic mass, which resided within the continuous epithelial-lined lumen in *A10ΔEC* females, but not in controls, where it resided within the embryonic crypt in the decidua (Fig. 6a, see diagram for orientation, embryos marked by an asterisk). Thus, lack of endothelial ADAM10 appears to affect embryonic crypt formation (Fig 6a).

Whole-mount imaging of 5.5 dpc implantation sites with Hypoxyprobe showed comparable levels of localized hypoxia in *A10ΔEC* females and controls (Fig. 6b, embryo marked by asterisk). In some cases, the embryonic mass also stained positive for hypoxyprobe in the mutant females, indicating possible metabolic stress prior to resorption of the implantation site at 5.5 dpc (Fig. 6b).

Comparable proliferation and distribution of immune cells in the implantation site of *A10ΔEC* mice at 5.5 dpc

To assess proliferation in the implantation site, we stained for the nuclear proliferation marker Ki67. Comparable numbers of Ki67-positive nuclei per total number of DAPI-stained nuclei were detected in the implantation sites of *A10ΔEC* and control females at 5.5 dpc (Fig. 7a, quantification in b). The endometrium (e) showed increased levels of Ki67 staining compared to the myometrium (m), excluding the area proximal to embryo implantation where Ki67-positive cells were rarely observed (Fig. 7a, site of decreased proliferation close to embryo implantation is enclosed by a dotted white line). Taken together, these results indicate that the loss of pregnancy in *A10ΔEC* females is most likely not caused by a lack of perfusion of decidual blood vessels or decreased cellular proliferation in the endometrium.

One of the roles of the decidua is to shield the implanting embryo from the maternal immune system [33]. To investigate possible defects in the appearance or distribution of maternal immune cells, we performed immunofluorescence staining for the pan-immune cell

marker CD45. There was no difference in distribution, localization or number of labeled cells in mutant versus control implantation sites at 5.5 dpc (Fig. 7c, quantification shown in d). As expected, immune cells localized predominately closer to the outer muscle layers. Similar results were obtained with the macrophage marker F4/80 (supplementary Fig. 5a). Finally, some vessels in the periphery of the endometrial tissue stained with the marker for lymphatic vessels LYVE1 in controls, whereas there were fewer endometrial LYVE1+ vessels in the mutants (supplementary Fig. 5b).

RNA-seq gene expression analysis of whole uterine horns at 5.5 dpc shows significant changes in markers for endothelial cells, for implantation and for decidualization.

In order to uncover potential changes in the molecular pathways that underly the pregnancy loss in *A10ΔEC* females, we performed RNA-seq analysis of the uterine horns from 3 separate mutant and control littermate pairs at 5.5 dpc. This uncovered 1058 differentially expressed genes, with 387 upregulated and 671 downregulated genes in *A10ΔEC* samples compared to controls (log2fold>1, P value <.01) (Fig. 8a). Pathway enrichment analysis showed significant upregulation of genes associated with angiogenesis, vasculogenesis and endothelial cell migration, while several of the most strongly downregulated genes were associated with mitochondrial function (supplementary Fig. 6a). Specifically, components of the Notch signaling pathway including the ligand *Dll4* and receptors *Notch1* and *Notch4*, were among the top upregulated genes (Fig. 8a), similar to what we found in coronary endothelial cells from *A10ΔEC* mice [29]. Moreover, we observed significant upregulation of *Kcne3*, a common marker for migratory tip-cells, which is upregulated upon inhibition of Notch signaling [34]. Furthermore, expression of *Snrk* and *Robo4* were upregulated, two genes that have been implicated in cell migration during angiogenesis [35–37]. In addition, genes associated with pathological neovascularization of the retina, including *Adora2a, Pparg* and *Ngfr* [38] were upregulated in mutant females.

The RNA-seq analysis also showed that genes expressed by uterine epithelial cells and genetic pathways required for implantation were expressed at higher levels in *A10ΔEC* females at 5.5dpc than in controls (Fig. 8a). Several of the differentially upregulated genes in *A10ΔEC* females are known to be essential for implantation in mice. Specifically *Lif* [39], *Sox9* [40] and *Foxa2* [8] are associated with glandular epithelium in the uterus, whereas *Cdh1* [41], *Msx1* [42], *Bmp7* [43] and *Muc1* [44] are expressed in uterine epithelial cells. Furthermore, we found reduced expression of markers of differentiated decidual cells, *Prl8a2* [45] and the Wnt inhibitor *Dkk1* [46], the latter of which is known to promote trophoblast invasion. Finally, we observed significantly decreased expression of genes associated with early embryonic development and differentiation of trophoblast cells, such as *Cts7, Cts8* [47], *Tbxt, Pfpl* [48], *Prl3d3 and Prl7b1* [49], consistent with impaired development of the embryo proper and extraembryonic trophoblasts preceding resorption of the implantation site (supplementary Fig. 6a,b).

RNA-seq of endometrial endothelial cells at 4.5 dpc shows decreased endothelial cell lineage commitment and suggests an interplay between Notch, Wnt and BMP signaling

To further investigate the role of endothelial ADAM10 in the establishment of pregnancy, we sorted endothelial cells (CD31+, CD45-) from the uterine horns of *A10ΔEC* and control

female littermates at 4.5 dpc for RNA-seq. We chose 4.5 dpc because at this stage, the endometrial vasculature still appears normal in mutant females and because the process of decidualization has not been initiated. This analysis uncovered downregulation of Notch target genes (Hey1, Hes1), consistent with a loss of Notch signaling (Fig. 8b, supplementary Fig. 6c,d). We also found upregulation of Notch1 and its ligand, Dll4, similar to the results of the 5.5 dpc endometrium (Fig. 8a,b). Endothelial cells from *A10ΔEC* females showed decreased expression of the arterial markers *Gja4* and *Hey1*, indicative of an immature "vein-like" arterial phenotype; which has been previously described upon blockage of the Notch pathway [29]. Two markers of immature endothelial cells, *Apln* and its receptor *AplnR* [50,51] were also upregulated, as were genes associated with endothelial cell differentiation, such as *Cd276* (B7-H3), *Cd34* and *Etv4* [52,53]. Furthermore, we found increased expression of the vasodilator peptide hormone *Adm*, a potential marker for preeclampsia, through 5.5 dpc. Finally, there was increased expression of *Bmp2*, *Bmp4*, *Bmp7* and *Tgfb1* and decreased expression of the TGFb accessory receptor Endoglin as well as of *Wnt11* and the Wnt pathway inhibitor *Dkk2*. The BMP and Wnt pathways have been implicated in uterine morphogenesis and decidualization, but endothelial cells have not previously been reported to contribute to these signaling pathways in the uterus [54–56].

Discussion

The main goal of this study was to investigate the potential causes for the severely reduced fertility of female *A10ΔEC* mice. We have uncovered an essential role for endothelial ADAM10, a crucial mediator of Notch signaling, in the establishment of a functional implantation site. In the absence of ADAM10, the endometrial endothelial cells are unable to support a normal decidualization reaction, resulting in loss of pregnancy. Previous studies have shown that endothelial ADAM10/Notch signaling is crucial for the development and maturation of specialized vascular structures, such as kidney glomeruli and coronary vessels [24,25]. The current study supports the notion that endometrial endothelial cells are part of a specialized vascular niche that requires ADAM10, and thus presumably Notch signaling, for the functional maturation of the endometrial vasculature during pregnancy.

Once we had established that *A10ΔEC* females are either infertile or highly subfertile, we were interested in determining the underlying cause. We found that implantation sites were present in the mutant animals after fertilization, initially at normal numbers at 4.5 dpc, then at slightly reduced numbers at 5.5 dpc, but that they were almost uniformly lost by 6.5 dpc. Thus, the lack of endothelial ADAM10 did not seem to directly affect fertilization or the initial stages of decidualization. Instead, most *A10ΔEC* females were unable to maintain a pregnancy, as evidenced by the resorption of the non-viable implantation sites by 6.5 dpc. The similar appearance of corpora lutei in *A10ΔEC* female mice and controls suggested that the defect was in the vasculature of the implantation site and not in the ovaries or in the vessels of the CL. Furthermore, the lack of major changes in estrogen and progesterone levels at 4.5 dpc and 5.5 dpc suggests that the loss of pregnancy was not caused by hormonal dysregulation, although this cannot be ruled out. This interpretation was further supported by the results of an artificial decidualization assay, in which the decidualization reaction was strongly reduced in *A10ΔEC* females, despite the absence of embryos. Previous studies in pigs showed that knocking down ADAM10 affects Trophoblast development, but such a

defect was not observed in *A10ΔEC* females because the Tie2-Cre inactivates ADAM10 in maternal endothelial cells [57].

Since the pregnancy loss in *A10ΔEC* female mice occurs between 5.5 and 6.5 dpc, we performed a histological and immunofluorescence analysis of the implantation site and a transcriptome analysis at this stage of pregnancy. This uncovered a failure to undergo a normal decidualization process within the endometrium of *A10ΔEC* mice, resulting in defective embryonic invasion and aberrant embryonic crypt formation. Importantly, the vasculature in the implantation sites of *A10ΔEC* females at 5.5dpc appeared abnormal, with enlarged vessels resembling veins in the center of the implantation site, which only had small capillaries in controls. These vessels were reminiscent of the enlarged and vein-like vessels seen in the retina of *A10ΔEC* mice, which are a well characterized manifestation of a lack of endothelial ADAM10/Notch signaling [24,25,14,17,13]. Nevertheless, the perfusion and the level of tissue hypoxia around the time of pregnancy loss appeared comparable in *A10ΔEC* females and controls, suggesting that the decreased decidualization is not caused by inadequate perfusion.

The transcriptional signature of the mutant compared to control implantation sites at 5.5 dpc showed an increase in the expression of genes associated with vascular signaling pathways as well as of genes associated with implantation. The increased expression of these pathways in mutant mice can presumably be explained by the persistence of a less differentiated state of the implantation site compared to controls at 5.5 dpc. As expected, genes associated with embryonic and trophoblast lineage development and decidualization were downregulated in the *A10ΔEC* female mice compared to controls, consistent with the observed loss of pregnancy. The gene expression profile of sorted uterine endothelial cells at 4.5 dpc further supported the notion that the functional differentiation of the endometrial endothelial cells is blocked or delayed in *A10ΔEC* female mice. Specifically, we found that markers for immature arterial precursors, such as *Gja4* and *AplnR,* were upregulated, as previously seen in the coronary vasculature of *A10ΔEC* mice [29]. Finally, the dysregulation of the Wnt and Bmp pathways in the endometrial vasculature suggested a potential interplay between ADAM10/Notch signaling and these pathways during pathological endometrial vascularization (Supplementary Fig. 5d). Some of the most upregulated genes in both the sorted EC population at 4.5 and whole uterus at 5.5 dpc were chromogranin A (Chga), apelin (Apln) and nitric oxide synthase-2 (Nos2). Chga is a member of the granin family that is expressed in secretory granules of neuroendocrine cells and serves as a precursor for signaling molecules such as vasostatin-1, which can have anti-angiogenic effects in tumors. The increased levels of Chga could therefore conceivably result in production secretory proteins such as vasostatin-1 that could contribute to the vascular defects in the mutant endometrium [58]. Nos2 is one of three Nos isoforms that is the most prevalent in the rat uterus during pregnancy [59] as well as in the mouse during early decidualization [60]. Female Nos2−/− mice are subfertile and have reduced vessel remodeling by midgestation [61]. Since upregulation of Nos2 in the deciduum in a preeclamptic mouse model (BPH/5) is thought to adversely affect pregnancy [62], the increased expression of Nos2 could also have a detrimental effect during early pregnancy in *A10ΔEC* mice. Finally, Apln, which is considered a marker for immature endothelial cells, was also elevated [50,51].

Taken together, these results support a model in which the inactivation of ADAM10 blocks a Notch-dependent cell fate decision in endometrial endothelial cells, resulting in an arrest or retention at a less mature state. Presumably, the *A10ΔEC* endothelial cells are unable to properly differentiate in response to the molecular and/or systemic cues of early pregnancy, such as from uterine dendritic cells (uDCs [63]). This results in aberrant vascular growth and remodeling, as evidenced by the presence of abnormally large vessels and an increase in markers for immature arterial endothelial cells within the implantation sites. Presumably, the immature endometrial endothelial cells are unable to support the differentiation of decidual cells, leading to abnormal implantation sites and the loss of pregnancy by 6.5 dpc. Although we feel that the most likely cause of the observed phenotypes is a lack of ADAM10/Notch-signaling in endometrial endothelial cells, we cannot rule out that other substrates of ADAM10, or other function of ADAM10 that are not related to its catalytic activity, cause the observed phenotypes. Overall, these findings point to a complex interplay of the different cell types that participate in the decidualization reaction to prepare the endometrium for implantation, with specialized endothelial cells playing a key role in this process.

In conclusion, this study has uncovered an essential role of endothelial ADAM10 in the earliest stages of pregnancy, i.e. in building a functional implantation site. Infertility caused by early pregnancy loss is a common pathology [64,65,5]. In mice, decidualization occurs exclusively upon implantation, but in ovulatory women the decidua is formed and shed monthly. By establishing a crucial role for endothelial cells early on in the implantation site, these studies could have implications for a better understanding of infertility by raising the possibility that endothelial cells are a potential cause of repeated pregnancy loss.

Materials and Methods

Mice

The female *A10ΔEC* mice were generated by mating adult female mice of mixed genetic background (129Sv/C57Bl6) containing two floxed alleles of ADAM10 but no *Tie2-Cre* transgene with adult males of mixed background containing two floxed alleles of ADAM10 and one allele of *Tie2Cre* [66], as previously described [24]. Previous studies have shown that mice with floxed alleles of ADAM10, but no Cre, are normal and indistinguishable from wild type mice [24] and that transgenic mice expressing only the *Tie2-Cre* are also normal, without any spontaneous pathological phenotypes [67]. The offspring containing two floxed alleles of ADAM10 and one allele of *Tie2Cre* are referred as *A10ΔEC* throughout this study, and mice carrying two floxed alleles of ADAM10 but no *Tie2-Cre* are referred to as controls. Female mice used for experiments were between 6–12 weeks and sexual receptivity was assessed prior to experiments based on vaginal appearance [68]. Littermates were used for all experiments, unless otherwise noted.

For timed matings, *A10ΔEC* or control adult females were mated with adult control males overnight. The following morning, the females were checked for the presence of a vaginal plug. If a plug was observed, females were separated from males and the afternoon after the vaginal plug was observed was considered 0.5 days post conception (dpc). To confirm pregnancy for experiments performed at 3.5 dpc, one uterine horn was flushed using a 27

Gauge needle filled with PBS. If blastocysts were present, the opposite uterine horn was further processed for experimental purposes.

For long-term fertility tracking experiments, two adult *A10ΔEC* or control females were placed in a cage with a control (two floxed alleles of ADAM10 but no *Tie2-Cre* transgene) or wildtype (129S1/SvImJ) male continuously for 4 months. Cages were checked regularly for pups. If pups were present, they were removed from the cage to allow for continuous mating. All animals were euthanized by administration of CO_2 according to the guidelines of the American Veterinary Association. All procedures were approved by the Animal Care and Use Committee of the Hospital for Special Surgery at Weill Cornell Medicine.

Immunohistochemistry and Histology

Three littermate pairs were sacrificed at the specified time points (3.5 dpc, 4.5 dpc and 5.5 dpc). Uterine horns were extracted and fixed overnight in 4% PFA. Following fixation, the tissue was gradually dehydrated overnight in 15% sucrose and in 30% sucrose. Tissue was embedded in Richard-Allan Scientific Neg50 (Thermo Fisher Scientific) and frozen at −80°C. Frozen tissue blocks were serial sectioned using a Cryostat CM3050 s (Leica Biosystems) in sections of 8 μm thickness.

For immunohistochemistry, sections were washed in PBS for 10 minutes at room temperature followed by blocking for one hour in 1% Normal Donkey Serum (Jackson ImmunoResearch, Inc., West Grove, PA) in 0.5% Triton X-100 and 0.1% Saponin in PBS (TSP). Sections were incubated for 1 hour with primary antibody, then washed 3x with PBS and incubated for 1 hour with secondary antibody. Sections were washed briefly 3 more times with PBS and incubated with DAPI solution for 5 minutes, followed by mounting with ProLong Diamond Antifade Mounting (#P36965, Invitrogen, Carlsbad, CA). All steps were performed in a 37°C humidified chamber, except washes and DAPI incubation, which were performed at room temperature (see supplemental Table for list of antibodies). For histology, frozen sections were stained using Hematoxylin & Eosin (H&E). Immunohistochemistry slides were imaged using a Zeiss LSM 710 confocal microscope and histology slides were imaged using a Nikon Eclipse 50i microscope.

Quantification of implantation site diameter

H&E images of at least 5 different sections of implantation sites at 5.5 dpc from 3 littermates were used for the quantification. Measurements of implantation site diameter were quantified using NIH ImageJ. For the diameter, a straight line was drawn on the endometrium along the longest distance within the antimesometrial-mesometrial axis. The length was referred to as d(a)), and a second line was drawn perpendicular to the first along the longest distance (referred to as d(b)). The diameter lengths were used to calculate the area of the implantation site using the formula to calculate the Area (A) of an ellipse A= pi ($\pi \times d(a)/2 \times d(b)/2$).

Quantification of immunofluorescence

Images were quantified using the colocalization function on ZEN Analysis Software (Zeiss). Only the endometrium was considered for quantification, the lumen of the epithelial luminal

layer as well as the embryonic crypt were excluded, if present. For calculations of CD31 relative area, 5 different sections per animal were quantified, from 3 littermate pairs at each timepoint (3.5, 4.5 and 5.5 dpc). To quantify immune cells and proliferation, slides from 3 littermates at 5.5 dpc were stained for the pan-immune cell marker CD45 or the proliferation marker Ki67 and DAPI. To approximate cell numbers, we quantified the fraction of immune cell nuclei (CD45+, DAPI+ area/Ki67+, DAPI+ area) to overall nuclei (DAPI), using masking colocalization analyses in three different sections per animal, from a total of 3 littermate pairs.

Alkaline Phosphatase Staining

Frozen sections of implantation sites at 5.5 dpc from three littermates were stained for alkaline phosphatase activity. Sections were incubated 2 times with NTMT (100mM NaCl, 100mM Tris-HCl pH9.5, 50mM MgCl2, 1% Tween20, 20μM Levamisole, in H2O) solution at room temperature for 10 minutes, followed by staining with NBT-BCIP (Roche) in NTMT for one hour in a humidified chamber at 37°C. After staining, the slides were washed with TSP for 10 minutes at room temperature and mounted with AquaMount Mounting medium (Thermo Fisher Scientific).

Determination of Serum Estrogen and Progesterone Levels

Adult control and *A10ΔEC* females were mated with control males and euthanized on day 4.5 dpc (n=5) or 5.5 dpc (n=4). Immediately after euthanasia blood was extracted from the left ventricle using a syringe with a 23G needle. The blood was left for an hour at room temperature to clot and centrifuged for 15 minutes at 2000 × g to allow for separation of the serum. Serum was collected and stored at −80° C until testing, which was performed by the University of Virginia Center for Research in Reproduction Ligand Assay and Analysis Core. Estrogen serum levels were measured using a Mouse/Rat Estradiol Elisa kit (Calbiotech, El Cajon, CA), and progesterone levels were measured using a Progesterone Mouse/Rat Elisa (IBL, Minneapolis, MN).

Artificial Decidualization:

Eight control and eight *A10ΔEC* females were mated with vasectomized wildtype males to induce pseudopregnancy. On day 3.5 dpc, females were briefly anesthetized with isoflurane and an incision was made on the lower back lateral to the midline to expose the right ovary and uterine horn. A 22G needle was inserted into the lumen of the right uterine horn from the proximal side closer to the oviduct and scratched along the anti-mesometrial side followed by suturing of the incision. The left horn was left untouched and served as an internal control. Females were sacrificed on 7.5bdpc and the uterus was dissected. To assess decidualization response, control and scratched uterine horns were weighed separately.

Retro-orbital Lectin Injections:

Three littermate pairs of adult females were briefly anesthetized using isoflurane at 5.5 dpc after mating with control males. 100 μl of a 10% solution of Dylight 649 labeled Lycopersicon Esculentum (Tomato) Lectin (Vector Laboratories, Burlingame CA) in PBS were injected retro-orbitally. Animals were sacrificed 5 minutes after injection. Uterine

horns were isolated and fixed overnight in 4% PFA at 4°C. Tissues were prepared for whole-mount imaging as described below.

Pontamine Sky Blue staining:

Five control and *A10ΔEC* females of reproductive age were mated with control males. At day 4.5 dcp after the copulation plug was observed the adult females were briefly anesthetized using isoflurane, and 100 μl of a 1% Pontamine (Chicago) Sky Blue 6B (Sigma-Aldrich) in PBS were injected retro-orbitally. Females were euthanized 3–5 minutes after the injection. The uterine horns were dissected and washed in PBS, to allow for counting of blue bands that marked the implantation sites along the uterine horns.

Hypoxyprobe:

Three littermate pairs of adult females at 5.5 dpc after mating with control males were intraperitoneally injected with Hypoxyprobe solution (Hypoxyprobe #HP7–100kit, Hypoxyprobe, Burlington, MA) at a concentration of 60mg/kg according to manufacturer's instructions. Animals were sacrificed one hour after the injection and the uterine horns were isolated and fixed in 4% PFA overnight at 4°C.

Tissue preparation for Whole-mount Imaging:

After overnight fixation of the uterine horns, single implantation sites were isolated for further processing. The tissue was blocked for 48 hrs in 5% NDS in PBS 0.01% Tween (PBS-T) in a shaking incubator at 37°C, followed by incubation with primary antibody for 48 hrs under the same conditions, then washed 3x in PBS-T for 30 minutes at room temperature. Subsequently, the tissue was incubated for 48 hrs with secondary antibody at 37°C shaking, followed by 3x washes in PBS-T for 30 minutes at room temperature. Then the tissue was gradually dehydrated using Methanol by immersion in the following solutions for 30 minutes at room temperature: 50% Methanol in PBS-T, 75% Methanol-in PBS-T and 3× 100% Methanol. Implantation sites were then gradually cleared in a 1:2 Benzyl Alcohol: Benzyl Benzoate solution (BABB) by incubating the tissue for 30 minutes at room temperature in 50% BABB in Methanol, 75% BABB in Methanol and 3x times in 100% BABB. Tissue was left overnight in 100% BABB solution. Images were taken in a Zeiss LSM 880 confocal microscope followed by processing using Imaris Software (Oxford Instruments).

Whole uterus RNA Extraction

Uterine horns of three adult littermate pairs were collected on 5.5 dpc after mating with a control male. Uterine horns were washed in ice-cold PBS and then the ovaries, oviduct, cervix and vagina were removed. RNA was extracted from the uterine horns using the RNeasy Plus Mini Kit (Qiagen #74104, Germantown, MD).

Isolation and Sorting of Uterine Endothelial Cells:

Uterine horns of two adult littermate pairs were collected on 4.5 dpc after mating with a control male. The uterine horns were dissected and placed in ice cold RPMI media containing 1% HEPES, 1% Penicilin-Streptomycin, 1% L-glutamine and 0.5% Bovine

Serum Albumin (BSA). Ovaries, oviduct and the cervix were removed and the remaining uterine horn was mechanically dissociated using blades. The minced tissue was placed in dissociation mix of the abovementioned media with collagenase type II, Dispase and DNAse I (Sigma) and incubated for 40 minutes at 37°C. After incubation, 0.5 mM EDTA was added and the tissue was further dissociated using a glass pipette. The remainder of the tissue was incubated for an additional 5 minutes at 37°C. The suspension was passed through a 70 μm filter and the flow through was centrifuged at 1,200 rpm for 5 minutes in an Eppendorf centrifuge (model 5702f). The cell pellet was resuspended and stained with Alexa Fluor 647 anti-mouse CD31 Antibody (# 102516, Biolegend), Alexa Fluor® 488 anti-mouse CD45 antibody (#103121, Biolegend) and DAPI for 20 minutes on ice. Endothelial cells (Cd31+, Cd45−, DAPI−) were sorted using a FACSJazz (BD Biosciences, San Jose, CA) cell sorter and RNA was immediately extracted using an Arcturus PicoPure RNA Isolation Kit (Applied Biosystems) according to the manufacturer's instructions.

RNA Sequencing and data processing:

Library preparation and RNA Sequencing was performed by the Weill Cornell Genomic Core Facility on whole uterus samples at 5.5 dpc and sorted endothelial cell samples at 4.5 dpc. The libraries were prepared using TruSeq Stranded mRNA Library Prep (Illumina, San Diego, Ca). Sequencing was done on an Illumina HiSeq4000 with 50 bp single-end reads.

RNA-seq data was aligned to the mouse reference genome mm10 using STAR with standard input parameters. Aligned reads were filtered for reads that mapped uniquely. Transcript counts were produced using HTseq against the Ensembl reference transcriptome. Transcript counts were normalized for library size and differential expression was determined using DESeq2 (Love et al., 2014). All downstream analyses and visualization of RNA-seq data were performed on variance-stabilizing transformed data obtained from DESeq2. Pathway Enrichment analysis was done using the Enrichr database.

For the sorted Endothelial Cells Samples were analyzed via the Digital Expression Explorer 2 pipeline [69] Docker container (https://hub.docker.com/r/mziemann/tallyup). The resulting gene counts were processed in R package edgeR [70] and a RPKM matrix was calculated after filtering and quality control.

Statistics and Graphs:

Statistical Analyses and Graphs were computed using Graphpad Prism 8. P values were calculated using unpaired two tailed t test and p values of less than 0.05 were deemed significant and noted as follows: p value *<0.05, **<0.01, ***< 0.001, ****<0.0001. For the artificial decidualization assay a paired two-tailed t test was used to determine the statistical significance of differences between the control and the scratched horn.

Supplementary Material

Refer to Web version on PubMed Central for supplementary material.

Acknowledgements.

We thank Dr. Laurie Lacko, Orla O'Shea, Dr. Tania Panellini, Dr. Kat Hadjantonakis, Dr. Gisela Weskamp and Dr. Dragos Dasoveanu for help, advice and insightful suggestions during the course of this project. The Weill Cornell Genomics core performed the RNA-seq analysis presented here. This study was funded in part by NIH R01 GM64750 and NIH R35 GM134907 to C. Blobel and by NIH R01 HL082098 and the March of Dimes Research Foundation (Research Grant #6-FY14–411) to H. Stuhlmann. G. Farber was funded by American Heart Association Predoctoral Fellowship (#17PRE33380001). The measurements of serum hormone levels were performed by The University of Virginia Center for Research in Reproduction Ligand Assay and Analysis Core which is supported by the Eunice Kennedy Shriver NICHD/NIH (NCTRI) Grant P50-HD28934.

References

1. Plaisier M (2011) Decidualisation and angiogenesis. Best Pract Res Clin Obstet Gynaecol 25 (3):259–271. doi:10.1016/j.bpobgyn.2010.10.011 [PubMed: 21144801]
2. Ramathal CY, Bagchi IC, Taylor RN, Bagchi MK (2010) Endometrial decidualization: of mice and men. Semin Reprod Med 28 (1):17–26. doi:10.1055/s-0029-1242989 [PubMed: 20104425]
3. Dey SK, Lim H, Das SK, Reese J, Paria BC, Daikoku T, Wang H (2004) Molecular cues to implantation. Endocr Rev 25 (3):341–373. doi:10.1210/er.2003-0020 [PubMed: 15180948]
4. Wang H, Dey SK (2006) Roadmap to embryo implantation: clues from mouse models. Nat Rev Genet 7 (3):185–199. doi:10.1038/nrg1808 [PubMed: 16485018]
5. Cha J, Sun X, Dey SK (2012) Mechanisms of implantation: strategies for successful pregnancy. Nat Med 18 (12):1754–1767. doi:10.1038/nm.3012 [PubMed: 23223073]
6. Fullerton PT Jr., Monsivais D, Kommagani R, Matzuk MM (2017) Follistatin is critical for mouse uterine receptivity and decidualization. Proc Natl Acad Sci U S A 114 (24):E4772–E4781. doi:10.1073/pnas.1620903114 [PubMed: 28559342]
7. Nallasamy S, Kaya Okur HS, Bhurke A, Davila J, Li Q, Young SL, Taylor RN, Bagchi MK, Bagchi IC (2019) Msx Homeobox Genes Act Downstream of BMP2 to Regulate Endometrial Decidualization in Mice and in Humans. Endocrinology 160 (7):1631–1644. doi:10.1210/en.2019-00131 [PubMed: 31125045]
8. Kelleher AM, Peng W, Pru JK, Pru CA, DeMayo FJ, Spencer TE (2017) Forkhead box a2 (FOXA2) is essential for uterine function and fertility. Proc Natl Acad Sci U S A 114 (6):E1018–E1026. doi:10.1073/pnas.1618433114 [PubMed: 28049832]
9. Afshar Y, Jeong JW, Roqueiro D, DeMayo F, Lydon J, Radtke F, Radnor R, Miele L, Fazleabas A (2012) Notch1 mediates uterine stromal differentiation and is critical for complete decidualization in the mouse. FASEB J 26 (1):282–294. doi:10.1096/fj.11-184663 [PubMed: 21990372]
10. Zhang S, Kong S, Wang B, Cheng X, Chen Y, Wu W, Wang Q, Shi J, Zhang Y, Wang S, Lu J, Lydon JP, DeMayo F, Pear WS, Han H, Lin H, Li L, Wang H, Wang YL, Li B, Chen Q, Duan E, Wang H (2014) Uterine Rbpj is required for embryonic-uterine orientation and decidual remodeling via Notch pathway-independent and - dependent mechanisms. Cell Res 24 (8):925–942. doi:10.1038/cr.2014.82 [PubMed: 24971735]
11. Su RW, Strug MR, Joshi NR, Jeong JW, Miele L, Lessey BA, Young SL, Fazleabas AT (2015) Decreased Notch pathway signaling in the endometrium of women with endometriosis impairs decidualization. J Clin Endocrinol Metab 100 (3):E433–442. doi:10.1210/jc.2014-3720 [PubMed: 25546156]
12. Shawber CJ, Lin L, Gnarra M, Sauer MV, Papaioannou VE, Kitajewski JK, Douglas NC (2015) Vascular Notch proteins and Notch signaling in the peri-implantation mouse uterus. Vasc Cell 7:9. doi:10.1186/s13221-015-0034-y [PubMed: 26629328]
13. Alabi RO, Farber G, Blobel CP (2018) Intriguing Roles for Endothelial ADAM10/Notch Signaling in the Development of Organ-Specific Vascular Beds. Physiol Rev 98 (4):2025–2061. doi:10.1152/physrev.00029.2017 [PubMed: 30067156]
14. Roca C, Adams RH (2007) Regulation of vascular morphogenesis by Notch signaling. Genes Dev 21 (20):2511–2524 [PubMed: 17938237]
15. Ehling M, Adams S, Benedito R, Adams RH (2013) Notch controls retinal blood vessel maturation and quiescence. Development 140 (14):3051–3061. doi:10.1242/dev.093351 [PubMed: 23785053]

16. Gridley T (2007) Notch signaling in vascular development and physiology. Development 134 (15):2709–2718 [PubMed: 17611219]
17. Gridley T (2010) Notch signaling in the vasculature. Curr Top Dev Biol 92:277–309. doi:10.1016/S0070-2153(10)92009-7 [PubMed: 20816399]
18. Hellstrom M, Phng LK, Hofmann JJ, Wallgard E, Coultas L, Lindblom P, Alva J, Nilsson AK, Karlsson L, Gaiano N, Yoon K, Rossant J, Iruela-Arispe ML, Kalen M, Gerhardt H, Betsholtz C (2007) Dll4 signalling through Notch1 regulates formation of tip cells during angiogenesis. Nature 445 (7129):776–780 [PubMed: 17259973]
19. Hofmann JJ, Iruela-Arispe ML (2007) Notch signaling in blood vessels: who is talking to whom about what? Circ Res 100 (11):1556–1568. doi:10.1161/01.RES.0000266408.42939.e4 [PubMed: 17556669]
20. Suchting S, Freitas C, le Noble F, Benedito R, Breant C, Duarte A, Eichmann A (2007) The Notch ligand Delta-like 4 negatively regulates endothelial tip cell formation and vessel branching. Proc Natl Acad Sci U S A 104 (9):3225–3230 [PubMed: 17296941]
21. Rooke J, Pan D, Xu T, Rubin GM (1996) KUZ, a conserved metalloprotease-disintegrin protein with two roles in Drosophila neurogenesis. Science 273 (5279):1227–1230 [PubMed: 8703057]
22. Hartmann D, de Strooper B, Serneels L, Craessaerts K, Herreman A, Annaert W, Umans L, Lubke T, Lena Illert A, von Figura K, Saftig P (2002) The disintegrin/metalloprotease ADAM 10 is essential for Notch signalling but not for alpha-secretase activity in fibroblasts. Hum Mol Genet 11 (21):2615–2624 [PubMed: 12354787]
23. Pan D, Rubin J (1997) KUZBANIAN controls proteolytic processing of NOTCH and mediates lateral inhibition during Drosophila and vertebrate neurogenesis. Cell 90:271–280 [PubMed: 9244301]
24. Glomski K, Monette S, Manova K, De Strooper B, Saftig P, Blobel CP (2011) Deletion of Adam10 in endothelial cells leads to defects in organ-specific vascular structures. Blood 118 (4):1163–1174. doi:10.1182/blood-2011-04-348557 [PubMed: 21652679]
25. Alabi RO, Glomski K, Haxaire C, Weskamp G, Monette S, Blobel CP (2016) ADAM10-Dependent Signaling Through Notch1 and Notch4 Controls Development of Organ-Specific Vascular Beds. Circ Res 119 (4):519–531. doi:10.1161/CIRCRESAHA.115.307738 [PubMed: 27354212]
26. Abrahamsohn PA (1983) Ultrastructural study of the mouse antimesometrial decidua. Anat Embryol (Berl) 166 (2):263–274. doi:10.1007/bf00305087 [PubMed: 6846860]
27. Finn CA, Hinchliffe JR (1964) Reaction of the Mouse Uterus during Implantation and Deciduoma Formation as Demonstrated by Changes in the Distribution of Alkaline Phosphatase. J Reprod Fertil 8:331–338. doi:10.1530/jrf.0.0080331 [PubMed: 14248593]
28. Zhao R, Wang A, Hall KC, Otero M, Weskamp G, Zhao B, Hill D, Goldring MB, Glomski K, Blobel CP (2014) Lack of ADAM10 in endothelial cells affects osteoclasts at the chondro-osseus junction. J Orthop Res 32 (2):224–230. doi:10.1002/jor.22492 [PubMed: 24108673]
29. Farber G, Parks MM, Lustgarten Guahmich N, Zhang Y, Monette S, Blanchard SC, Di Lorenzo A, Blobel CP (2019) ADAM10 controls the differentiation of the coronary arterial endothelium. Angiogenesis 22 (2):237–250. doi:10.1007/s10456-018-9653-2 [PubMed: 30446855]
30. dela Paz NG, D'Amore PA (2009) Arterial versus venous endothelial cells. Cell Tissue Res 335 (1):5–16. doi:10.1007/s00441-008-0706-5 [PubMed: 18972135]
31. Kusumbe AP, Ramasamy SK, Adams RH (2014) Coupling of angiogenesis and osteogenesis by a specific vessel subtype in bone. Nature 507 (7492):323–328. doi:10.1038/nature13145 [PubMed: 24646994]
32. Kuhn A, Brachtendorf G, Kurth F, Sonntag M, Samulowitz U, Metze D, Vestweber D (2002) Expression of endomucin, a novel endothelial sialomucin, in normal and diseased human skin. J Invest Dermatol 119 (6):1388–1393. doi:10.1046/j.1523-1747.2002.19647.x [PubMed: 12485444]
33. Erlebacher A (2013) Immunology of the maternal-fetal interface. Annu Rev Immunol 31:387–411. doi:10.1146/annurev-immunol-032712-100003 [PubMed: 23298207]
34. Zhao Q, Eichten A, Parveen A, Adler C, Huang Y, Wang W, Ding Y, Adler A, Nevins T, Ni M, Wei Y, Thurston G (2018) Single-Cell Transcriptome Analyses Reveal Endothelial Cell Heterogeneity in Tumors and Changes following Antiangiogenic Treatment. Cancer Res 78 (9):2370–2382. doi:10.1158/0008-5472.CAN-17-2728 [PubMed: 29449267]

35. Lu Q, Xie Z, Yan C, Ding Y, Ma Z, Wu S, Qiu Y, Cossette SM, Bordas M, Ramchandran R, Zou MH (2018) SNRK (Sucrose Nonfermenting 1-Related Kinase) Promotes Angiogenesis In Vivo. Arterioscler Thromb Vasc Biol 38 (2):373–385. doi:10.1161/ATVBAHA.117.309834 [PubMed: 29242271]
36. Suchting S, Heal P, Tahtis K, Stewart LM, Bicknell R (2005) Soluble Robo4 receptor inhibits in vivo angiogenesis and endothelial cell migration. FASEB J 19 (1):121–123. doi:10.1096/fj.04-1991fje [PubMed: 15486058]
37. Bedell VM, Yeo SY, Park KW, Chung J, Seth P, Shivalingappa V, Zhao J, Obara T, Sukhatme VP, Drummond IA, Li DY, Ramchandran R (2005) roundabout4 is essential for angiogenesis in vivo. Proc Natl Acad Sci U S A 102 (18):6373–6378. doi:10.1073/pnas.0408318102 [PubMed: 15849270]
38. Liu Z, Yan S, Wang J, Xu Y, Wang Y, Zhang S, Xu X, Yang Q, Zeng X, Zhou Y, Gu X, Lu S, Fu Z, Fulton DJ, Weintraub NL, Caldwell RB, Zhang W, Wu C, Liu XL, Chen JF, Ahmad A, Kaddour-Djebbar I, Al-Shabrawey M, Li Q, Jiang X, Sun Y, Sodhi A, Smith L, Hong M, Huo Y (2017) Endothelial adenosine A2a receptor-mediated glycolysis is essential for pathological retinal angiogenesis. Nat Commun 8 (1):584. doi:10.1038/s41467-017-00551-2 [PubMed: 28928465]
39. Kimber SJ (2005) Leukaemia inhibitory factor in implantation and uterine biology. Reproduction 130 (2):131–145. doi:10.1530/rep.1.00304 [PubMed: 16049151]
40. Gonzalez G, Mehra S, Wang Y, Akiyama H, Behringer RR (2016) Sox9 overexpression in uterine epithelia induces endometrial gland hyperplasia. Differentiation 92 (4):204–215. doi:10.1016/j.diff.2016.05.006 [PubMed: 27262401]
41. Reardon SN, King ML, MacLean JA 2nd, Mann JL, DeMayo FJ, Lydon JP, Hayashi K (2012) CDH1 is essential for endometrial differentiation, gland development, and adult function in the mouse uterus. Biol Reprod 86 (5):141, 141–110. doi:10.1095/biolreprod.112.098871 [PubMed: 22378759]
42. Nallasamy S, Li Q, Bagchi MK, Bagchi IC (2012) Msx homeobox genes critically regulate embryo implantation by controlling paracrine signaling between uterine stroma and epithelium. PLoS Genet 8 (2):e1002500. doi:10.1371/journal.pgen.1002500 [PubMed: 22383889]
43. Monsivais D, Clementi C, Peng J, Fullerton PT Jr., Prunskaite-Hyyrylainen R, Vainio SJ, Matzuk MM (2017) BMP7 Induces Uterine Receptivity and Blastocyst Attachment. Endocrinology 158 (4):979–992. doi:10.1210/en.2016-1629 [PubMed: 28324064]
44. Meseguer M, Pellicer A, Simon C (1998) MUC1 and endometrial receptivity. Mol Hum Reprod 4 (12):1089–1098. doi:10.1093/molehr/4.12.1089 [PubMed: 9872358]
45. Roby KF, Deb S, Gibori G, Szpirer C, Levan G, Kwok SC, Soares MJ (1993) Decidual prolactin-related protein. Identification, molecular cloning, and characterization. J Biol Chem 268 (5):3136–3142 [PubMed: 7679108]
46. Peng S, Li J, Miao C, Jia L, Hu Z, Zhao P, Li J, Zhang Y, Chen Q, Duan E (2008) Dickkopf-1 secreted by decidual cells promotes trophoblast cell invasion during murine placentation. Reproduction 135 (3):367–375. doi:10.1530/REP-07-0191 [PubMed: 18299430]
47. Screen M, Dean W, Cross JC, Hemberger M (2008) Cathepsin proteases have distinct roles in trophoblast function and vascular remodelling. Development 135 (19):3311–3320. doi:10.1242/dev.025627 [PubMed: 18776147]
48. Kashiwagi A, DiGirolamo CM, Kanda Y, Niikura Y, Esmon CT, Hansen TR, Shioda T, Pru JK (2007) The postimplantation embryo differentially regulates endometrial gene expression and decidualization. Endocrinology 148 (9):4173–4184. doi:10.1210/en.2007-0268 [PubMed: 17510242]
49. Simmons DG, Rawn S, Davies A, Hughes M, Cross JC (2008) Spatial and temporal expression of the 23 murine Prolactin/Placental Lactogen-related genes is not associated with their position in the locus. BMC Genomics 9:352. doi:10.1186/1471-2164-9-352 [PubMed: 18662396]
50. Kidoya H, Takakura N (2012) Biology of the apelin-APJ axis in vascular formation. J Biochem 152 (2):125–131. doi:10.1093/jb/mvs071 [PubMed: 22745157]
51. Farber G, Hurtado R, Loh S, Monette S, Mtui J, Kopan R, Quaggin S, Meyer-Schwesinger C, Herzlinger D, Scott RP, Blobel CP (2018) Glomerular endothelial cell maturation depends

on ADAM10, a key regulator of Notch signaling. Angiogenesis 21 (2):335–347. doi:10.1007/s10456-018-9599-4 [PubMed: 29397483]

52. Son Y, Kwon SM, Cho JY (2019) CD276 (B7-H3) Maintains Proliferation and Regulates Differentiation in Angiogenic Function in Late Endothelial Progenitor Cells. Stem Cells 37 (3):382–394. doi:10.1002/stem.2944 [PubMed: 30379377]
53. Xu R, Chen W, Zhang Z, Qiu Y, Wang Y, Zhang B, Lu W (2018) Integrated data analysis identifies potential inducers and pathways during the endothelial differentiation of bone-marrow stromal cells by DNA methyltransferase inhibitor, 5-aza-2'-deoxycytidine. Gene 657:9–18. doi:10.1016/j.gene.2018.03.010 [PubMed: 29514045]
54. Tepekoy F, Akkoyunlu G, Demir R (2015) The role of Wnt signaling members in the uterus and embryo during pre-implantation and implantation. J Assist Reprod Genet 32 (3):337–346. doi:10.1007/s10815-014-0409-7 [PubMed: 25533332]
55. Goad J, Ko YA, Kumar M, Syed SM, Tanwar PS (2017) Differential Wnt signaling activity limits epithelial gland development to the anti-mesometrial side of the mouse uterus. Dev Biol 423 (2):138–151. doi:10.1016/j.ydbio.2017.01.015 [PubMed: 28153546]
56. Zhang S, Lin H, Kong S, Wang S, Wang H, Wang H, Armant DR (2013) Physiological and molecular determinants of embryo implantation. Mol Aspects Med 34 (5):939–980. doi:10.1016/j.mam.2012.12.011 [PubMed: 23290997]
57. Kwon J, Jeong SM, Choi I, Kim NH (2016) ADAM10 Is Involved in Cell Junction Assembly in Early Porcine Embryo Development. PLoS One 11 (4):e0152921. doi:10.1371/journal.pone.0152921 [PubMed: 27043020]
58. Mahata SK, Corti A (2019) Chromogranin A and its fragments in cardiovascular, immunometabolic, and cancer regulation. Ann N Y Acad Sci 1455 (1):34–58. doi:10.1111/nyas.14249 [PubMed: 31588572]
59. Ali M, Buhimschi I, Chwalisz K, Garfield RE (1997) Changes in expression of the nitric oxide synthase isoforms in rat uterus and cervix during pregnancy and parturition. Mol Hum Reprod 3 (11):995–1003. doi:10.1093/molehr/3.11.995 [PubMed: 9433927]
60. Cameron IT, Campbell S (1998) Nitric oxide in the endometrium. Hum Reprod Update 4 (5):565–569. doi:10.1093/humupd/4.5.565 [PubMed: 10027610]
61. Burnett TG, Tash JS, Hunt JS (2002) Investigation of the role of nitric oxide synthase 2 in pregnancy using mutant mice. Reproduction 124 (1):49–57. doi:10.1530/rep.0.1240049 [PubMed: 12090918]
62. Heyward CY, Sones JL, Lob HE, Yuen LC, Abbott KE, Huang W, Begun ZR, Butler SD, August A, Leifer CA, Davisson RL (2017) The decidua of preeclamptic-like BPH/5 mice exhibits an exaggerated inflammatory response during early pregnancy. J Reprod Immunol 120:27–33. doi:10.1016/j.jri.2017.04.002 [PubMed: 28432903]
63. Plaks V, Birnberg T, Berkutzki T, Sela S, BenYashar A, Kalchenko V, Mor G, Keshet E, Dekel N, Neeman M, Jung S (2008) Uterine DCs are crucial for decidua formation during embryo implantation in mice. J Clin Invest 118 (12):3954–3965. doi:10.1172/JCI36682 [PubMed: 19033665]
64. Sapra KJ, Joseph KS, Galea S, Bates LM, Louis GM, Ananth CV (2017) Signs and Symptoms of Early Pregnancy Loss. Reprod Sci 24 (4):502–513. doi:10.1177/1933719116654994 [PubMed: 27342274]
65. Salker M, Teklenburg G, Molokhia M, Lavery S, Trew G, Aojanepong T, Mardon HJ, Lokugamage AU, Rai R, Landles C, Roelen BA, Quenby S, Kuijk EW, Kavelaars A, Heijnen CJ, Regan L, Macklon NS, Brosens JJ (2010) Natural selection of human embryos: impaired decidualization of endometrium disables embryo-maternal interactions and causes recurrent pregnancy loss. PLoS One 5 (4):e10287. doi:10.1371/journal.pone.0010287 [PubMed: 20422017]
66. Kisanuki YY, Hammer RE, Miyazaki J, Williams SC, Richardson JA, Yanagisawa M (2001) Tie2-Cre transgenic mice: a new model for endothelial cell-lineage analysis in vivo. Dev Biol 230 (2):230–242 [PubMed: 11161575]
67. Weskamp G, Mendelson K, Swendeman S, Le Gall S, Ma Y, Lyman S, Hinoki A, Eguchi S, Guaiquil V, Horiuchi K, Blobel CP (2010) Pathological Neovascularization Is Reduced by

Inactivation of ADAM17 in Endothelial Cells but Not in Pericytes. Circ Res 106 (5):932–940 [PubMed: 20110534]

68. Allen E (1922) The oestrous cycle in the mouse. American J of Anatomy 30:297–371
69. Ziemann M, Kaspi A, El-Osta A (2019) Digital expression explorer 2: a repository of uniformly processed RNA sequencing data. Gigascience 8 (4). doi:10.1093/gigascience/giz022
70. Robinson MD, McCarthy DJ, Smyth GK (2010) edgeR: a Bioconductor package for differential expression analysis of digital gene expression data. Bioinformatics 26 (1):139–140. doi:10.1093/bioinformatics/btp616 [PubMed: 19910308]

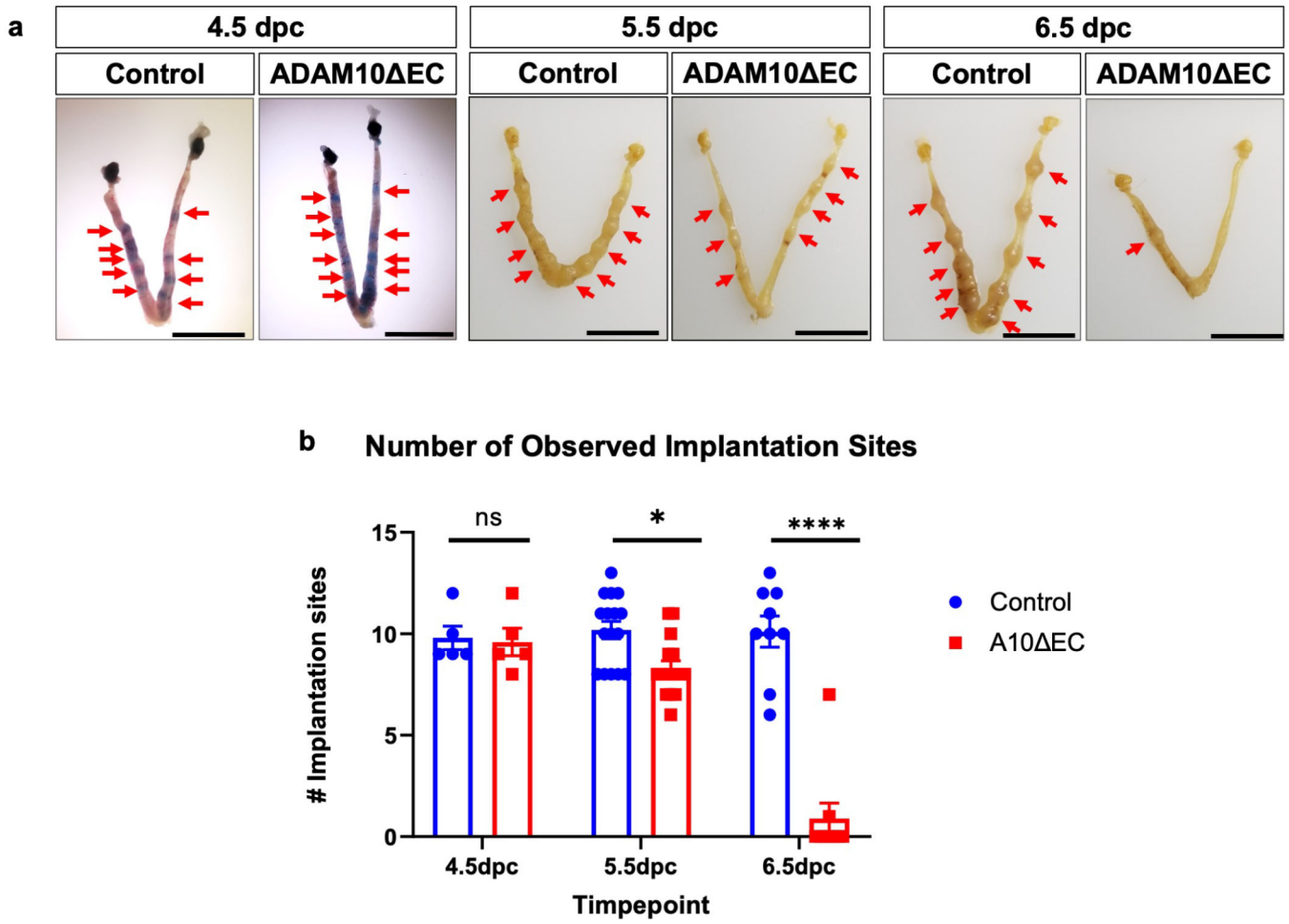

Fig. 1. Pregnancy loss in *A10ΔEC* females occurs between 5.5 dpc and 6.5 dpc

a) Implantation sites (marked with arrows) are clearly present in both control and *A10ΔEC* female mice at 4.5 and 5.5 dpc, whereas most or all implantation sites of the mutant females are completely resorbed at 6.5 dpc (one implantation site remains in the image shown here). Representative images, scale bar = 1cm. b) Quantification of the number of implantation sites in *A10ΔEC* females at 4.5 dpc (n=5 per genotype), 5.5 dpc (n=15 per genotype)and 6.5 dpc (n=9 per genotype), * indicates p≤0.05; **** indicates p≤0.0001; ns, not significant.

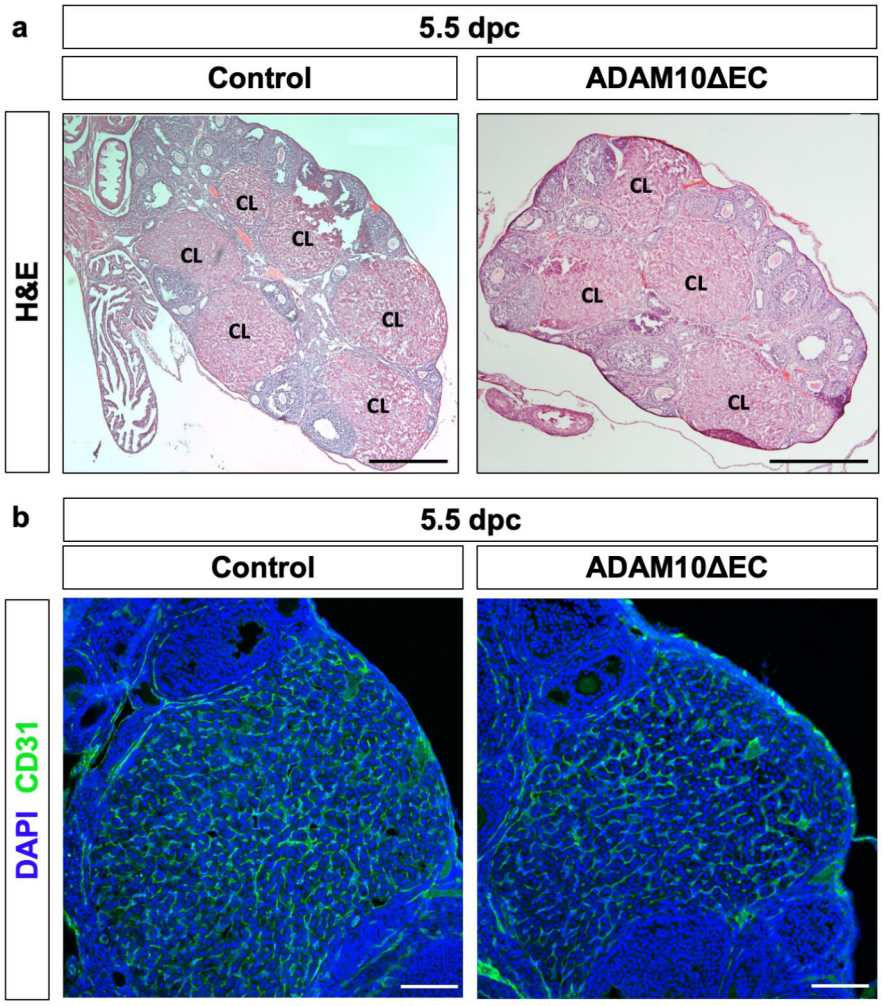

Fig. 2. At the time of pregnancy loss the appearance of the corpora lutea and their vasculature is normal in *A10ΔEC* females

a) H&E staining of whole ovaries shows comparable morphology in *A10ΔEC* females and controls at 5.5 dpc. CL=Corpus Luteum. Scale bar 500μm. b) Immunofluorescence staining of a representative CL at 5.5 dpc for the pan-endothelial cell marker CD31 shows successful vascularization of the CL and normal endothelial cell patterning. Scale Bar 100μm. Panels c and d are representative for sections from 3 separate animals, with 5 sections per animal.

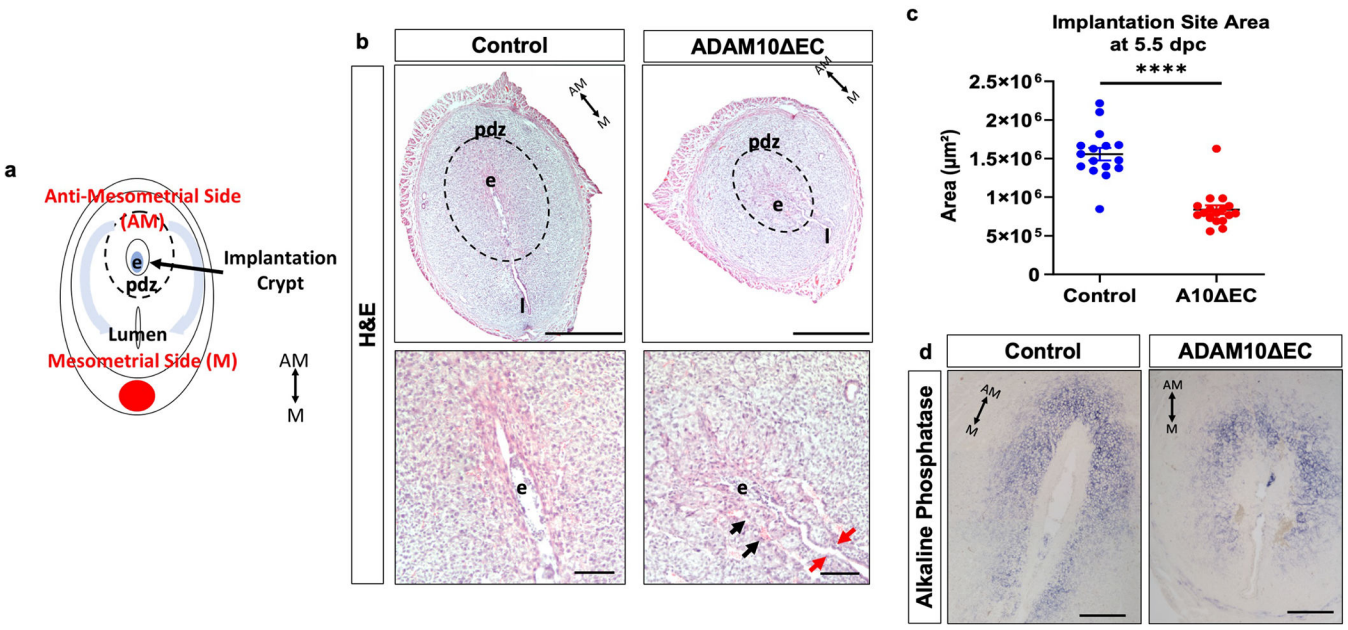

Fig. 3. The decidualization reaction in *A10ΔEC* females is impaired

a) Diagram of a transverse section of an implantation site, depicting the directionality of the decidualization reaction in a light blue arrow, from the antimesometrial (AM) to the mesometrial (M) side of the uterus; e=embryo, pdz= primary decidual zone, surrounded by dotted line; red dot, main blood vessel. b) H&E staining of implantation sites at the same time point illustrates the decreased diameter of the overall implantation site and dense proximal decidual zone in mutant females (top panels). Higher magnification images of the embryonic crypt show incomplete closure (red arrow), accompanied by large red blood cell filled spaces (black arrow) and a less developed embryonic body in *A10ΔEC* implantation sites (bottom panel). e= embryo, dotted line/pdz=primary decidual zone, l= lumen. Scale bar (top) 500μm, (bottom)100 μm. c) The area of the endometrial fraction of the implantation sites at 5.5dpc defined *as* $A = \pi * r(a) * r(b)$ is significantly reduced in mutant females (n=3, ≥5 sections/animal). **** indicates p ≤0.0001. d) Alkaline phosphatase (AP) staining of 5.5 dpc implantation sites shows that stromal fibroblast can differentiate into AP-positive decidual cells in *A10ΔEC* females, although the cells appear disorganized compared to the control. Scale bar 100μm.

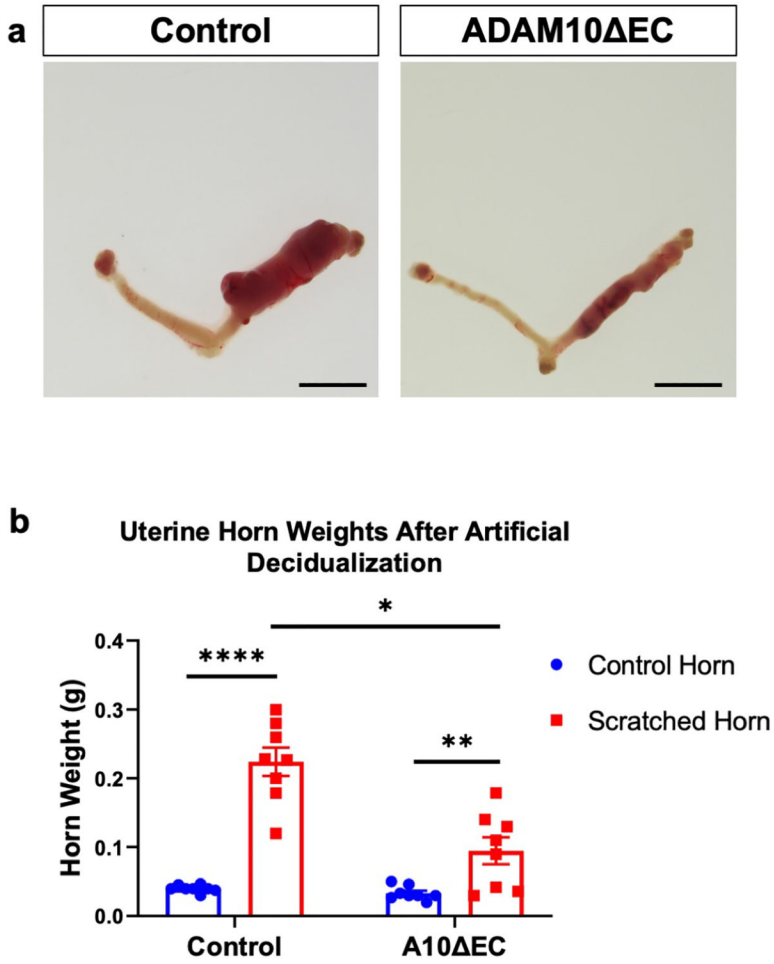

Fig. 4. Artificial decidualization model recapitulates impaired decidualization response in *A10ΔEC* females

a) *A10ΔEC* females show an attenuated response to artificial decidualization induced by mechanical stimulation of the uterine horn in pseudopregnant females (right horn), with the opposite horn serving as an internal control (left horn). Scale bar 1cm. b) Comparison of weights of the control horn and the scratched horn show significantly lower weight of the scratched horns in *A10ΔEC* females compared to controls; n=8. * indicates $p \leq 0.05$, ** $p \leq 0.01$, **** $p \leq 0.0001$.

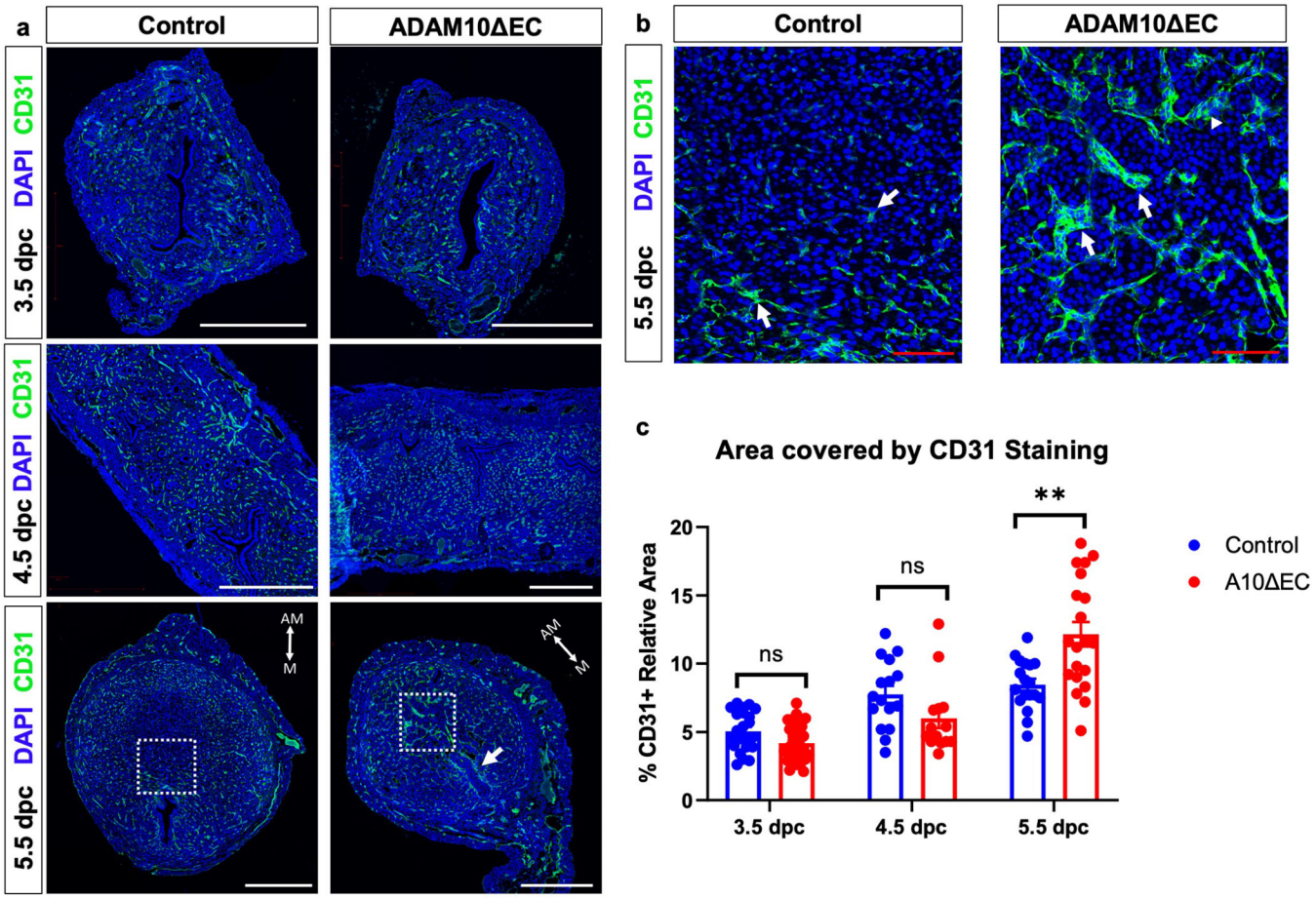

Fig. 5. *A10ΔEC* females display an abnormal vasculature and increased CD31 staining during the initiation of decidualization (5.5 dpc)

a) Progression of the vascularization of uterine horns at 3.5 dpc, 4.5 dpc, and 5.5 dpc visualized by immunofluorescence staining for CD31. Scale bars 500μm. Dotted squares in the 5.5 dpc samples identify the area shown in the enlarged images of the decidual area in panel b), where the abnormal appearance of the vasculature is most evident. White arrows identify capillaries in the control images and abnormal large caliber vessels in mutants. Scale bars represent 100um. c) Quantification of the CD31+ area in the implantation sites *A10ΔEC* females shows a significant increase at the onset of abnormal vascular patterning at 5.5 dpc (n=3; 5 sections per animal, ** indicates p≤0.001).

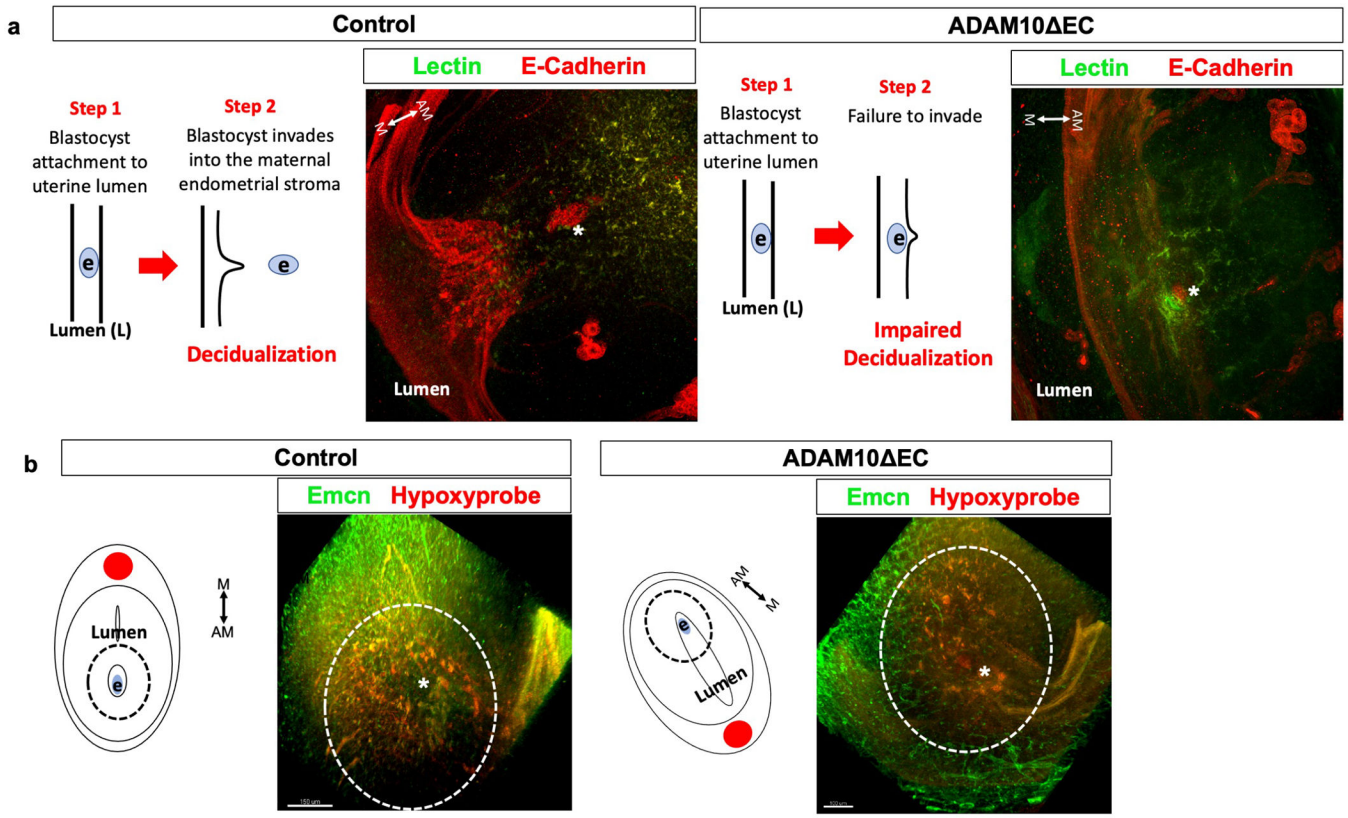

Fig. 6. Whole-mount imaging of implantation sites at 5.5 dpc to assess tissue perfusion and levels of hypoxia

a) Whole-mount imaging of implantation sites of females that had been retro-orbitally injected with fluorescently labeled *tomato lectin*. The samples were also stained with the epithelial marker E-cadherin. The lectin staining suggests that the vasculature at the endometrial implantation site of mutant females is adequately perfused. *A10ΔEC* mice showed increased lectin deposition close to the site of embryo implantation. b) Whole-mount imaging of implantation sites of females intraperitoneally injected with Hypoxyprobe show that hypoxia levels were comparable between control and mutant females at 5.5 dpc. Both show localized hypoxia surrounding the implantation site, which is indicated by an oval dotted line. Diagrams of cross sections of implantation sites indicate the orientation of image. Scale bar 100μm (n=3). * marks the position of the embryo in a and b.

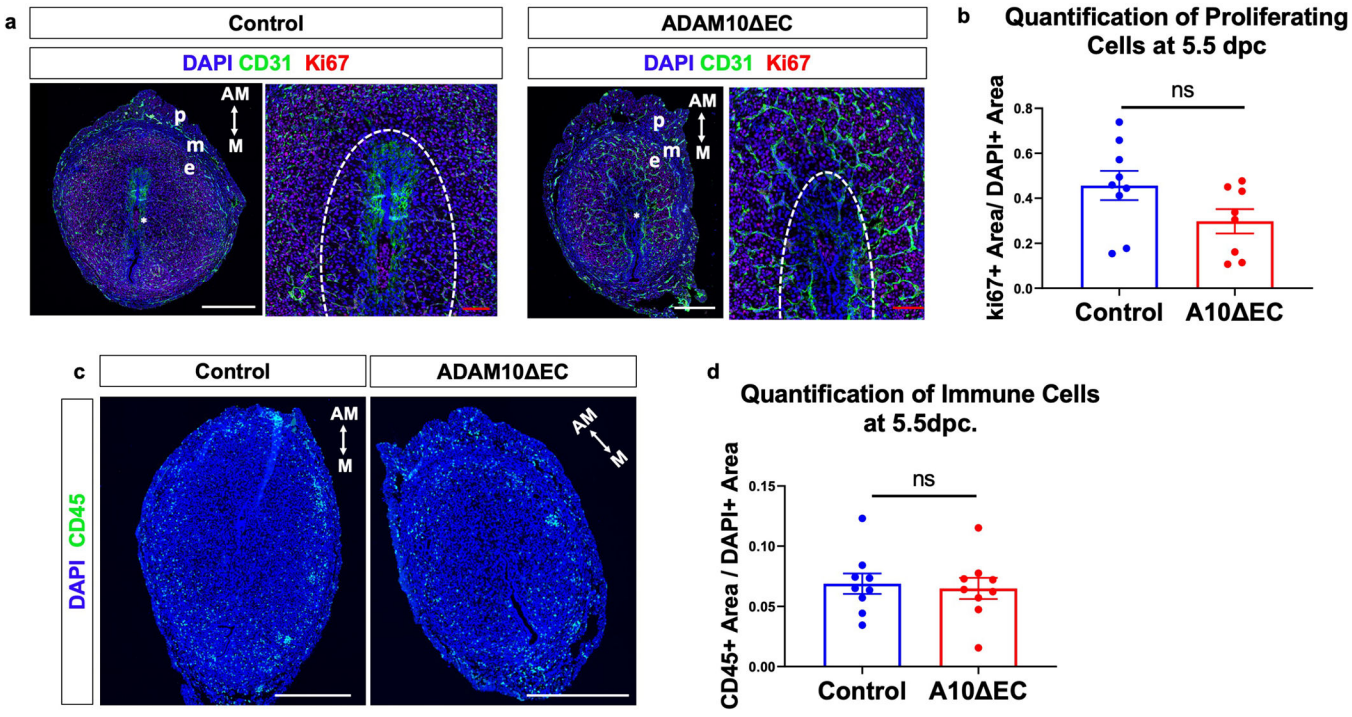

Fig. 7. Immunofluorescence staining of 5.5 dpc implantation sites show comparable levels and patterning of proliferating cells as well as immune cells

Assessment of proliferation in the implantation sites at 5.5 dpc via immunofluorescence staining with the proliferation maker Ki67. The samples were also stained with the endothelial marker CD31 to highlight the vasculature. Scale bar 500μm. The proliferation patterning is similar in mutant and control implantation sites. In both cases, there was moderate proliferation in the perimetrium (p), decreased proliferation in the myometrium (m) and increased in proliferation in the periphery of the endometrium (e); while the area surrounding the embryonic implantation sites was mostly non-proliferative. Magnified images shown in the right panel, Scale bar 100μm (n=3; 5 sections per animal) b) Quantification of proliferative cells in the endometrium shows no significant difference between *A10ΔEC* females and controls. c) The staining pattern of immune cells shows no difference between mutant and control females. (Scale bar 500μm, n=3, 5 sections per animal, quantification in d).

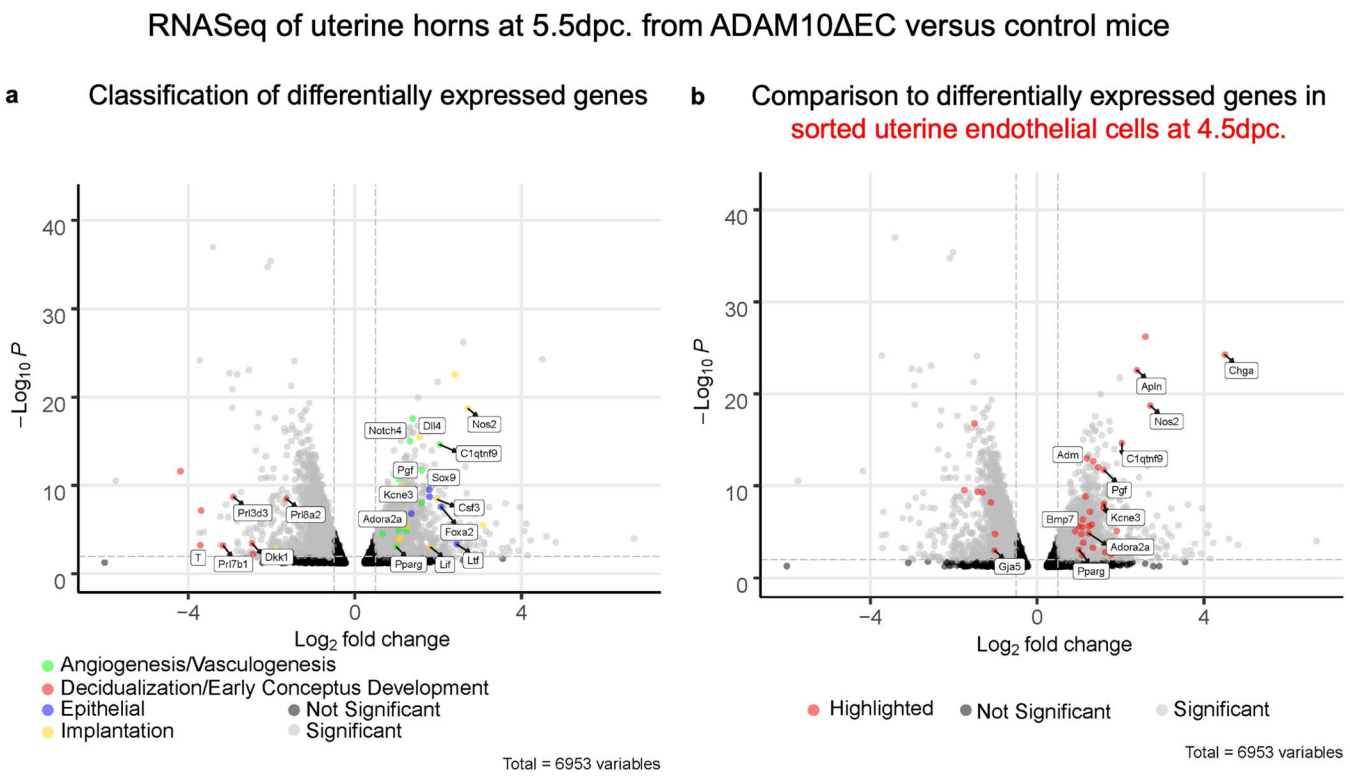

Fig. 8. RNASeq of whole uterine horns shows differential expression of key genes associated with endothelial cells, or with implantation or decidualization

a) A Volcano plot of differentially expressed genes in whole uterine horns at 5.5 dpc shows upregulation of genes associated with endothelial cells (green dots), genes associated with implantation (yellow dots) and genes canonically expressed by uterine epithelial cells (purple) in *A10ΔEC* females compared to controls; while key genes associated to embryonic development and decidualization (red dots) are downregulated in mutant compared to control females. b) The volcano plot in panel b is essentially the same as the one in panel a, except that differentially expressed genes in sorted endothelial cells at 4.5 dpc are highlighted that were also found to be dysregulated in whole uterine horns at 5.5 dpc.

Table 1.

Fertility of *A10ΔEC* females compared to controls

Mating Scheme(♀×♂)	Females	Females that gave birth	Pups	Pups per female (average)	Litters	Pups per litter (average)
Control × Control	8	8	183	22.88 ± 3.1	23	9.96 ± 2.2
ADAM10ΔEC × Control	8	2	19	2.3 ± 4.4	6	3.18± 0.8
ADAM10ΔEC × Wildtype	5	2	8	1.6 ± 2.6	3	2.7 ±2.1